Molecular Pharmacology Fast Forward. Published on June 24, 2013 as doi:10.1124/mol.113.087320
This article has not been copyedited and formatted. The final version may differ from this version.

Reverse engineering of the selective agonist, TBPB, unveils both orthosteric and allosteric modes of action at the M_1 muscarinic acetylcholine receptor

Peter Keov, Celine Valant, Shane M. Devine, J. Robert Lane, Peter J. Scammells, Patrick M. Sexton, Arthur Christopoulos

Drug Discovery Biology & Department of Pharmacology (P.K., C.V., J.R.L., P.M.S., A.C.), and Medicinal Chemistry (S.M.D., P.J.S.), Monash Institute of Pharmaceutical Sciences, Monash University, Parkville

Molecular Pharmacology Fast Forward. Published on June 24, 2013 as DOI: 10.1124/mol.113.087320
This article has not been copyedited and formatted. The final version may differ from this version.

Running title: Characterisation of a bitopic mode of action of TBPB

Corresponding author:

Prof. Arthur Christopoulos, Drug Discovery Biology, Monash Institute of Pharmaceutical Sciences, Monash University, Parkville, Victoria, 3052, Australia. Tel: +613 9903 9067. Fax: +613 9903 9581

Email: arthur.christopoulos@monash.edu

Number of text pages: 27

Number of tables: 5

Number of figures: 10

Number of references: 42

Number of words in the Abstract: 240

Number of words in the Introduction: 747

Number of words in the Discussion: 1484

Molecular Pharmacology Fast Forward. Published on June 24, 2013 as DOI: 10.1124/mol.113.087320
This article has not been copyedited and formatted. The final version may differ from this version.

Abbreviations

AC-42, 4-*n*-butyl-1-[4-(2-methylphenyl)-4-oxo-1-butyl]-piperidine hydrogen chloride; 77-LH-28-1, 1-[3-(4-butyl-1-piperidinyl)propyl]-3,4-dihydro-2(1*H*)-quinolinone; TBPB, 11-(1'-(2-methylbenzyl)-1,4'-bipiperidin-4-yl)-1*H*-benzo[*d*]imidazol-2(3*H*)-one; BSA, bovine serum albumin; CHO, Chinese Hamster ovary; DMEM, Dulbecco's modified Eagle medium; ERK1/2, extracellular signal-regulated kinase 1 & 2; GPCR, G protein-coupled receptor; GppNHp, guanosine-5′-(βγ-imido)triphosphate; HBS, HEPES buffered saline; C_7/3-phth, heptane-1,7-bis-[dimethyl-3'-phthalimidopropyl]-ammonium bromide; $[Ca^{2+}]_i$, intracellular calcium; mAChR, muscarinic acetylcholine receptor; McN-A-343, 4-(*N*-(3-chlorophenyl)carbamoyloxy)-2-butynyltrimethylammonium chloride; [^{3}H]NMS, [^{3}H]*N*-methylscopolamine; VCP794, 1-(1-cyclohexylpiperidin-4-yl)-1*H*-benzo[*d*]imidazol-2(3*H*)-one (18); VCP813, *N*,*N*-Dimethyl-1-(2-methylbenzyl)piperidin-4-amine

Molecular Pharmacology Fast Forward. Published on June 24, 2013 as DOI: 10.1124/mol.113.087320
This article has not been copyedited and formatted. The final version may differ from this version.

Abstract

Recent interest in the M_1 muscarinic acetylcholine (ACh) receptor (mAChR) has led to the discovery of various selective agonists for the receptor. The novel selective agonist, 1-(1'-(2-methylbenzyl)-1,4'-bipiperidin-4-yl)-1*H*-benzo[*d*]imidazol-2(3*H*)-one (TBPB), displays unprecedented functional selectivity at the M_1 mAChR. This functional selectivity has been described to stem from sole interaction with an allosteric site, although the evidence for such a mechanism is equivocal. To delineate TBPB's mechanism of action, several truncated variants of TBPB were synthesised and characterised. Binding experiments with [^{3}H]-*N*-methylscopolamine ([^{3}H]-NMS) at the M_1, M_2, M_3 and M_4 mAChRs revealed radioligand displacement in a manner consistent with a competitive binding mode at the orthosteric site by TBPB and fragment derivatives. Cell-based functional assays of fragment derivatives of TBPB identified both agonistic and antagonistic moieties, one of which, 1-(1-cyclohexylpiperidin-4-yl)-1*H*-benzo[*d*]imidazol-2(3*H*)-one (18) (VCP794), lost agonistic selectivity for the M_1 mAChR. Further interaction experiments between TBPB or its antagonist fragments with ACh also indicated a mechanism consistent with competitive binding at mAChRs. However, interaction with an allosteric site by an antagonist fragment of TBPB was demonstrated via its ability to retardation radioligand dissociation. To reconcile this dual orthosteric/allosteric pharmacological behaviour, we propose that TBPB is a bitopic ligand, interacting with both the orthosteric site and an allosteric site, at the M_1 mAChR. This mechanism may also be the case for other selective agonists for mAChRs, and should be taken into consideration in the profiling and classification of new novel selective agonists for this receptor family.

Molecular Pharmacology Fast Forward. Published on June 24, 2013 as DOI: 10.1124/mol.113.087320
This article has not been copyedited and formatted. The final version may differ from this version.

Introduction

The muscarinic acetylcholine (ACh) receptors (mAChRs) are prototypical rhodopsin-like G protein-coupled receptors (GPCRs) that mediate a range of physiological processes within the central nervous system and the periphery. Of the five mAChR subtypes, the M_1 mAChR is involved in cognition and memory (Langmead et al., 2008b), and is a promising therapeutic target for treating a range of disorders such as Alzheimer's disease and schizophrenia. Indeed, the M_1/M_4 mAChR preferring agonist, xanomeline, showed clinically positive outcomes in studies of patients with both disorders (Bodick et al., 1997; Shekhar et al., 2008). However, the high occurrence of adverse side effects in subjects, attributed predominantly to actions at peripheral M_2 and M_3 mAChRs, exemplifies the challenge of developing subtype-selective compounds that target the highly homologous ACh-binding (orthosteric) site shared across the mAChR family.

Allosteric modulation of mAChRs is now well appreciated (Christopoulos et al., 1993; Clark and Mitchelson, 1976; Conn et al., 2009; Stockton et al., 1983). Upon binding to a site on the receptor that is topographically distinct from the orthosteric site, allosteric ligands modulate orthosteric ligand affinity and/or efficacy. Allosteric sites can also be less conserved across a GPCR family, offering potential to develop subtype selective compounds (Keov et al., 2011). As such, recent studies have discovered several highly subtype-selective mAChR allosteric modulators (Chan et al., 2008; Ma et al., 2009; Marlo et al., 2009).

In the search for selective activators of the M_1 mAChR, a number of ligands have been classified as "allosteric" agonists (Jones et al., 2008; Langmead et al., 2008a; Lebois et al., 2010; Spalding et al., 2002). However, whether these compounds convey their actions solely via an allosteric

Molecular Pharmacology Fast Forward. Published on June 24, 2013 as DOI: 10.1124/mol.113.087320
This article has not been copyedited and formatted. The final version may differ from this version.

site or via interaction with the orthosteric site remains uncertain. One such recently identified M_1 mAChR-selective agonist, TBPB (Figure 1), displays high functional selectivity for the M_1 mAChR, yet the current evidence to support an allosteric mode of action remains equivocal. For example, previously reported non-competitive antagonism between TBPB and atropine observed in a calcium mobilization assay (Jones et al., 2008), may reflect a hemi-equilibrium state (Charlton and Vauquelin, 2010) rather than allostery. Similarly, functional insensitivity of TBPB to mutation of the orthosteric residue, $Y381^{6.51}A$ (Jones et al., 2008; Ward et al., 1999), may be reconciled with either an allosteric mode of binding or simply a different binding pose within the orthosteric pocket. Importantly, TBPB has been shown to retard the dissociation of the orthosteric antagonist, [^{3}H]-*N*-methylscopolamine (NMS) from the M_1 mAChR (Jacobson et al., 2010), which is an important hallmark of allosteric interaction. However, this assay reflects interaction of a test ligand on a receptor that has been pre-equilibrated with orthosteric antagonist; although suggesting that TBPB can adopt an allosteric pose under such a circumstance, it does not guarantee that the ligand will adopt an allosteric mode of binding if the orthosteric site is unoccupied (Avlani et al., 2010).

Similar behaviours have been reported of the M_1 mAChR-selective agonists 4-*n*-butyl-1-[4-(2-methylphenyl)-4-oxo-1-butyl]piperidine hydrogen chloride (AC-42) and 1-[3-(4-butyl-1-piperidinyl)propyl]-3,4-dihydro-2(1*H*)-quinolinone (77-LH-28-1) (Langmead et al., 2008a; Spalding et al., 2002). We have demonstrated that AC-42 and 77-LH-28-1, despite not engaging with some amino acid residues required by prototypical agonists, can occupy the orthosteric domain of the M_1 and M_2 mAChRs in addition to, or simultaneously with the allosteric site via a bitopic mechanism (Avlani et al., 2010; May et al., 2007). Such a mechanism was first demonstrated for (4-(*N*-(3-chlorophenyl)carbamoyloxy)-2-butynyltrimethylammonium chloride

(McN-A-343) at the M_2 mAChR. We previously adopted a reverse engineering approach to delineate its mechanism, by truncating McN-A-343 to identify distinct orthosteric and allosteric pharmacophores (Valant et al., 2008).

Given the potential mixed orthosteric/allosteric characteristics of TBPB, similar to AC-42 and 77-LH-28-1, we hypothesised that TBPB is a bitopic ligand, rather than a pure allosteric agonist. Recent studies by Digby et al. (2012) and Sheffler et al. (2013) have made similar proposals, but remained unclear as to whether this mechanism involved concomitant binding to both orthosteric and allosteric sites, or acting as pure allosteric ligands at low concentrations and recognizing the orthosteric site only at higher concentrations. Such distinctions are important, because ascertaining differences between classes of ligands at the preclinical stage of discovery is vital in improving the likelihood of clinical translation of such molecules. Thus, to investigate this for TBPB, we adopted a reverse engineering approach. We provide evidence consistent with TBPB interacting concomitantly with orthosteric and allosteric sites in a bitopic mode of action and show distinct structural moieties required by TBPB for interaction with the orthosteric binding domain and an allosteric site at the M_1 mAChR.

Molecular Pharmacology Fast Forward. Published on June 24, 2013 as DOI: 10.1124/mol.113.087320
This article has not been copyedited and formatted. The final version may differ from this version.

Materials and Methods

Materials

Chinese hamster ovary (CHO) Flp-In cells and Fluo-4-AM were purchased from Invitrogen (Carlsbad, CA). Dulbecco's modified Eagle medium (DMEM) and fetal bovine serum (FBS) were from Gibco (Gaithersburg, MD) and JRH Biosciences (Lenexa, KS), respectively. The AlphaScreen SureFire phospho-ERK1/2 reagents were kindly donated by Drs. Michael Crouch and Ron Osmond (TGR Biosciences, South Australia, Australia). The AlphaScreen streptavidin donor beads and anti-IgG (protein A) acceptor beads used for phosphorylated ERK1/2 detection and [^{3}H]-*N*-methylscopolamine ([^{3}H]-NMS; specific activity, 85.4 Ci/mmol) were purchased from PerkinElmer Life and Analytical Sciences (Waltham, MA). TBPB and its fragment derivatives, VCP794 and *N*,*N*-Dimethyl-1-(2-methylbenzyl)piperidin-4-amine (VCP813), were synthesized in-house as described in the Supplementary Information. All other chemicals were from Sigma Chemical Co. (St. Louis, MO).

cDNA Constructs and Generation of Stable Cell Line

cDNA encoding the wild-type human M_1 (M_1) muscarinic acetylcholine receptor (mAChR) was obtained from Missouri University of Science and Technology (http://www.cdna.org) and was provided in pcDNA3.1+. Sequence of the hM_1 mAChR was amplified by PCR and cloned into the Gateway entry vector pENTR/D-TOPO, using the pENTR directional TOPO cloning kit, according to the manufacturer's instructions (Invitrogen). The construct was subsequently transferred into the Gateway destination vector pEF5/frt/V5/dest using the LR Clonase enzyme

Molecular Pharmacology Fast Forward. Published on June 24, 2013 as DOI: 10.1124/mol.113.087320
This article has not been copyedited and formatted. The final version may differ from this version.

mix (Invitrogen), and the constructs were used to transfect Flp-In CHO cells (Invitrogen) as described previously (May et al., 2007). Cells were selected using 600μg/ml (for the M_1 mAChR) hygromycin B (Roche) to generate cell lines stably expressing each receptor construct. Cells expressing the wild-type human M_2, M_3 and M_4 mAChRs were generated previously (May et al., 2007; Nawaratne et al., 2008; Stewart et al., 2010).

Cell Culture and Membrane Preparations

Cells were maintained and cultured in high glucose DMEM (Gibco) containing 10% FBS, 16 mM HEPES, and 600μg/ml hygromycin B at 37°C under a humidified atmosphere containing 5% CO_2. Membranes of cells expressing the M_1, M_2, M_3 and M_4 mAChR were generated as previously described (Nawaratne et al., 2008), except that the final pellet was resuspended in 5mL of buffer (20mM HEPES, 0.1mM EDTA, pH7.4).

Radioligand Binding assays

Binding assays were conducted as per Valant, *et al.* (2008). In all experiments, each reaction used 5μg of membrane expressing the M_1 mAChR (B_{max} = 4.01±0.93pmol/mg), or with 15μg, 10μg and 5μg of membranes expressing the M_2 (B_{max} = 2.44±0.15pmol/mg), M_3 (B_{max} = 5.83±2.01pmol/mg) or M_4 mAChR (B_{max} = 9.26±0.18pmol/mg), respectively. Briefly, in the case of equilibrium binding experiments, membranes were incubated with an approximate equilibrium dissociation constant (K_D) concentration of [^{3}H]-NMS and varying concentrations of test compound in 1mL buffer (100mM NaCl, 10mM $MgCl_2$, 20mM HEPES, pH 7.4) at 30°C or 37°C for 1-1.5h, depending on the subtype. [^{3}H]-NMS binding in the presence of varying

Molecular Pharmacology Fast Forward. Published on June 24, 2013 as DOI: 10.1124/mol.113.087320
This article has not been copyedited and formatted. The final version may differ from this version.

concentrations of test compound was determined in the presence of 100μM guanosine-5′-(βγ-imido)triphosphate (GppNHp).

Similar conditions were used for [^{3}H]-NMS dissociation kinetic experiments. Membranes expressing the M_1 mAChR were pre-equilibrated with [^{3}H]-NMS for 60min at 37°C, followed by dissociation of the bound radioligand initiated with atropine (10μM) alone or in the presence of a single concentration of each ligand – TBPB (100μM), VCP813 (300μM), VCP794 (100μM) or C_7/3-phth (100μM) – added in a reverse time course protocol at time points ranging from 1min to 15min.

Non-specific binding was determined in the presence of 10μM atropine for all studies. Reactions were terminated by rapid filtration onto GF/B grade filter paper (Whatman, Maidstone, UK) using a Brandel harvester, followed by three washes with ice-cold NaCl (0.9%). Radioactivity was determined via liquid scintillation counting.

Measurement of Intracellular Extracellular Signal Regulated Kinase 1 & 2 (ERK1/2) phosphorylation

For all experiments, cells were seeded onto transparent 96-well cell culture plates at 4 X 10^4cells per well for M_1 mAChR expressing cells and 3 X 10^4cells per well for cells expressing M_2, M_3 and M_4 mAChRs. Cells were grown overnight until confluent. Stimulation of ERK1/2 phosphorylation was determined using the AlphaScreen ERK1/2 SureFire protocol (TGR Biosciences). Prior to assay, cells were washed twice with 200μL PBS and incubated in serum-free DMEM (supplemented with 16mM HEPES) for at least 4h at 37°C in 5% CO_2. The assay was performed at 37°C followed by addition of ligand to cells to a final volume of 200μL. Time

course experiments were initially performed to determine the time at which maximal ERK1/2 phosphorylation occurred following agonist stimulation. For subsequent agonist-stimulated concentration-response experiments, cells were incubated with each agonist for the time required to achieve peak response (3-5 minutes). For functional interaction studies, concentration-response curves were constructed for ACh in the absence and presence of varying concentrations of the reference orthosteric antagonist, atropine, TBPB or VCP813. Compounds were pre-incubated for 30min prior to addition of ACh, except when intrinsic agonism was detected, whereby co-addition with ACh was conducted instead.

Ligand stimulated ERK1/2 phosphorylation was terminated by removal of media and drugs, followed by addition of 100μL per well SureFire™ lysis buffer and agitation of lysates for 5min at room temperature. 5μL of this lysate was added in a 384-well white Proxiplate™ (Perkin Elmer). A mixture of SureFire™ activation buffer, SureFire™ reaction buffer and AlphaScreen™ beads was prepared in a ratio of 100:600:3 (v/v/v) and added to the lysate for a lysate:mixture ratio of 5:8 (v/v). Plates were incubated for 1-1.5h at 37°C before the florescence signal was measured on a Fusion-α™ plate reader (PerkinElmer) using standard Alphascreen™ settings.

For all experiments, 10% FBS was used as an internal positive control to stimulate pERK1/2 (peak response at 3min for M_1 mAChR or 5min for other subtypes), whilst vehicle was used as negative control.

Intracellular Calcium ($[Ca^{2+}]_i$) Mobilisation

Molecular Pharmacology Fast Forward. Published on June 24, 2013 as DOI: 10.1124/mol.113.087320
This article has not been copyedited and formatted. The final version may differ from this version.

Cells expressing the M_1 mAChR were cultured overnight on transparent 96-well cell culture plates at 4 X 10^4cells per well. At the time of assay, cells were washed once using HEPES buffered saline (HBS) solution (150mM NaCl, 2.2mM $CaCl_2$, 2.6mM KCl, 1.18mM $MgCl_2$, 10mM HEPES, 10mM D-glucose) containing 0.5% bovine serum albumin (BSA) and 4mM Probenecid, at pH 7.4. Cells were then treated with (1μM) Fluo-4-AM (in HBS/BSA/Probenecid) for 60 min at 37°C in 5% CO_2 in the dark. Cells were then further washed (2 times) and placed in 180μL HBS/BSA/Probenecid solution. Ligands were added to cells in a FLEXstation 3 plate reader (Molecular Devices). For interaction studies, ligands were added simultaneously to cells. Ca^{2+}/Fluo-4 fluorescence was then measured in the FLEXstation at an excitation wavelength of 485nm and an emission wavelength of 525nm, for 100s (16s prior to and 84s following addition of ligand) at 37°C.

Data Analysis

All data were analysed using Graphpad Prism 5.02 (Graphpad Software, San Diego, CA). For radioligand saturation binding data, non-specific and total binding data were globally fitted to the following equation (equation 1):

$$Y = \frac{B_{max} \times [A]}{[A] \times K_D} + NS \times [A] \quad (1)$$

where Y is the total binding, B_{max} is the total receptor density, $[A]$ is the radioligand concentration, K_D is the equilibrium dissociation constant of radioligand and NS is non-specific radioligand binding. Data were expressed as picomoles of bound radioligand per mg of protein.

Molecular Pharmacology Fast Forward. Published on June 24, 2013 as DOI: 10.1124/mol.113.087320
This article has not been copyedited and formatted. The final version may differ from this version.

pK_D ± S.E. and B_{max} ± S.E. values were determined from 3 separate experiments performed in triplicate.

For radioligand inhibition binding experiments, data sets for each ligand were fitted to a one-site binding equation and two-site binding equation to estimate inhibitor potency, followed by F-test analysis to determine which equation best fitted the data (Nawaratne et al., 2008). Equilibrium dissociation constant values, K_i, were subsequently derived from inhibition binding experiments using the Cheng-Prusoff equation (Cheng and Prusoff, 1973).

For radioligand dissociation kinetics experiments, data sets for each treatment were fitted to a single phase exponential decay equation (May et al., 2007), with estimated dissociation rate constants (K_{off}) statistically compared to incubation with atropine alone via F-test.

Agonist concentration-response curves from $[Ca^{2+}]_i$ mobilisation and ERK1/2 phosphorylation experiments were fitted to the a four-parameter-logistic-equation to derive estimates for agonist potencies (pEC_{50}) and maximal agonist responses (E_{max}). For antagonist-mediated agonist concentration-response curve shifts, data of concentration-response curves in the absence and presence of antagonist were fitted to a Schild regression analysis (Arunlakshana and Schild, 1959).

The quantification of signalling bias was determined by nonlinear regression analysis of agonist concentration-response curves of $[Ca^{2+}]_i$ mobilisation and ERK1/2 phosphorylation, using a form

Molecular Pharmacology Fast Forward. Published on June 24, 2013 as DOI: 10.1124/mol.113.087320
This article has not been copyedited and formatted. The final version may differ from this version.

of the operational model of agonism as described by Kenakin et al. (2012) and Kenakin and Christopoulos (2013) (equation 2),

$$Y = Basal + \frac{(E_m - Basal)\times(\frac{\tau}{K_A})^n \times [A]^n}{[A]^n \times (\frac{\tau}{K_A})^n + \left(1 + \frac{[A]}{K_A}\right)^n} \quad (2)$$

where E_m is the maximal attainable system response for the given pathway, Basal is the level of response in the absence of agonist, τ is defined by the ratio of the total concentration of receptors to the concentration of agonist receptor-complex that produces half the maximal system response, K_A denotes the functional equilibrium dissociation constant of the agonist for the receptor, n is the slope of the transducer function that links occupancy with response. The ratio of τ/K_A (determined as a single fitted parameter - the logarithm $Log_{10}(\tau/K_A)$) is referred herein to as the "transduction coefficient", and incorporates both the affinity of the agonist for the active (signalling) state of the receptor and the efficiency of receptor coupling to signalling mechanisms.

Following estimation of the transduction coefficient for each agonist at each signalling pathway, the $Log_{10}(\tau/K_A)$ values were normalised to that determined for the endogenous agonist, ACh, within each signalling pathway, in order to cancel cell-dependent effects on the agonism observed for each pathway. This yields a "normalised transduction coefficient", denoted as $\Delta Log_{10}(\tau/K_A)$, calculated as (equation 3)

$$\Delta Log_{10}\left(\frac{\tau}{K_A}\right) = Log_{10}\left(\frac{\tau}{K_A}\right)_{test} - Log_{10}\left(\frac{\tau}{K_A}\right)_{ACh} \quad (3)$$

The determination of a ligand's actual agonist bias towards one pathway (j1) over another (j2) is given as (equation 4)

Molecular Pharmacology Fast Forward. Published on June 24, 2013 as DOI: 10.1124/mol.113.087320
This article has not been copyedited and formatted. The final version may differ from this version.

$$Bias = 10^{\Delta\Delta Log_{10}\left(\frac{\tau}{K_A}\right)_{j1-j2}} \quad (4)$$

where (equation 5)

$$\Delta\Delta Log_{10}\left(\frac{\tau}{K_A}\right) = Log_{10}(Bias) = \Delta Log_{10}\left(\frac{\tau}{K_A}\right)_{j1} - \Delta\Delta Log_{10}\left(\frac{\tau}{K_A}\right)_{j2} \quad (5)$$

Biased signalling is detected when Bias values are not significantly different from 1, otherwise observed when Log_{10}(Bias) values are significantly different from zero. Due to the determination of composite parameters, the associated propagation of error in equations 3-5 was accounted through application of the following equation (equation 6)

$$Pooled\ SE = \sqrt{(SE1)^2 + (SE2)^2} \quad (6)$$

Statistical analyses were performed, as appropriate, using Student's t test or one-way ANOVA with Dunnett's or Bonferroni's post-tests, and significance taken as $p < 0.05$.

Molecular Pharmacology Fast Forward. Published on June 24, 2013 as DOI: 10.1124/mol.113.087320
This article has not been copyedited and formatted. The final version may differ from this version.

Results

Evidence for competitive interaction with the orthosteric binding site by TBPB

The binding of TBPB to membranes of Flp-In CHO cells expressing the M_1 mAChR was investigated using equilibrium binding studies. TBPB inhibited in a concentration-dependent manner the binding of 1.0nM [^{3}H]-NMS ($pK_D = 8.93 \pm 0.09$) from the M_1 mAChR (Figure 2A), as did ACh. This behaviour is consistent with a competitive mode of interaction with the receptor, with the displacement of radioligand similar to that of the orthosteric ligands, ACh and atropine. As such, the data were empirically fitted to a one-site inhibitory mass action curve to determine potency (IC_{50}) estimates, followed by conversion to equilibrium binding dissociation constant estimates (Table 1).

The ability of TBPB to bind to other mAChR subtypes was additionally investigated. Equilibrium binding studies conducted on membranes expressing the M_2, M_3 and M_4 mAChRs revealed TBPB-mediated inhibition of [^{3}H]-NMS binding at all subtypes investigated (Figure 2B-D). The binding affinities of TBPB estimated at these subtypes were also comparable, with an approximately 3-fold maximal divergence (M_1 vs. M_2).

We next studied the functional activity of TBPB at the M_1, M_2, M_3 and M_4 mAChRs. Despite differences in Gα subtype coupling preferences, activation of each of the M_1 - M_4 mAChR subtypes results in convergent signalling to ERK1/2 phosphorylation (Crespo et al., 1994; Rosenblum et al., 2000). Hence, we chose to investigate mAChR-mediated ERK1/2 phosphorylation. As expected, TBPB robustly activated M_1 mAChR-mediated phosphorylation of ERK1/2 (Figure 3A, Table 2). TBPB failed to elicit responses at the M_2 and M_3 mAChRs, but

Molecular Pharmacology Fast Forward. Published on June 24, 2013 as DOI: 10.1124/mol.113.087320
This article has not been copyedited and formatted. The final version may differ from this version.

behaved as a weak partial agonist at the M_4 mAChR subtype, mediating ERK1/2 phosphorylation with sub-micromolar potency, comparable to its affinity previously estimated at this subtype (Figure 3B-D).

Given the lack of agonist activity of TBPB at the M_2 and M_3 mAChRs and reduced efficacy observed at the M_4 subtype, we investigated the antagonist properties of this ligand (Figure 4). Consistent with the competitive-like displacement of [^{3}H]-NMS observed at these receptors, TBPB antagonised ACh-mediated responses, characterized by a parallel, dextral displacement of the endogenous agonist's concentration-response curve. TBPB antagonism of ACh at the M_2 and M_3 mAChR was well fitted by the Schild model, with the estimated Schild slopes close to unity (Table 3).

Evidence for interaction with an allosteric site by TBPB

Although we have found evidence for TBPB competitively interacting with the orthosteric ligands of mAChRs, we examined whether TBPB could also interact allosterically with the M_1 mAChR, as per its initial classification as an allosteric agonist (Jones et al., 2008). Kinetic binding experiments are perhaps the best suited experiments to confirm allosteric interactions (Christopoulos et al., 1998). The modulation of the rate of [^{3}H]-NMS dissociation from M_1 mAChRs (K_{off} = 0.231 ± 0.005 min^{-1}) would be demonstrative of interaction of with an allosteric site. For instance, the prototypical allosteric modulator, C_7/3-phth, significantly retards [^{3}H]-NMS dissociation (K_{off} = 0.019 ± 0.002 min^{-1}, p<0.05, F test vs atropine alone; Figure 5). Consistent with previous reports (Jacobson et al., 2010), the presence of TBPB (100μM) modestly but significantly retarded [^{3}H]-NMS dissociation, compared to dissociation in the presence of atropine (10μM) alone, from the M_1 mAChR (K_{off} = 0.201 ± 0.005 min^{-1}, p<0.05, F

Molecular Pharmacology Fast Forward. Published on June 24, 2013 as DOI: 10.1124/mol.113.087320
This article has not been copyedited and formatted. The final version may differ from this version.

test vs atropine alone), demonstrating TBPB is able to interact allosterically with the [^{3}H]-NMS-bound receptor.

Truncation of TBPB unmasks a biased agonist and an antagonist fragment

The dual orthosteric/allosteric pharmacology of TBPB suggests that this novel ligand could be bitopic. We have previously adopted a reverse engineering approach to elucidate the roles of structural moieties for the binding and function of the bitopic agonist, McN-A-343, at the M_2 mAChR (Valant et al., 2008), therefore we truncated TBPB to further investigate its mechanism of action at the M_1 mAChR. A range of fragment molecules were synthesised representing truncations from both the "upper" *ortho*-tolyl end and "lower" benzoimidazolone end of TBPB. These fragments were subsequently screened for their abilities to activate or antagonise M_1 mAChR-mediated $[Ca^{2+}]_i$ mobilisation and ERK1/2 phosphorylation in Flp-In CHO cells, from which two fragment compounds were identified, VCP794 and VCP813, each representing truncation from either the *ortho*-tolyl end or the benzoimidazolone end, respectively (Figure 1).

VCP794 exhibited robust agonist activity for both $[Ca^{2+}]_i$ mobilisation and ERK1/2 phosphorylation, maximally activating receptor-mediated responses to the same levels as the endogenous agonist, ACh, and the parent molecule, TBPB (Figure 6A&B). When comparing the potency values of each agonist between the two different functional outputs, it appeared that all three agonists ACh, TBPB and VCP794 exhibited bias towards $[Ca^{2+}]_i$ mobilisation relative to ERK1/2 phosphorylation. However, intriguingly, whilst VCP794 exhibited approximately a 3-fold lower potency than TBPB in $[Ca^{2+}]_i$ mobilisation experiments, the fragment compound displayed an approximately 3-fold higher potency than TBPB in ERK1/2 phosphorylation experiments. Such reversal of potency values is indicative of biased agonism, meaning the

Molecular Pharmacology Fast Forward. Published on June 24, 2013 as DOI: 10.1124/mol.113.087320
This article has not been copyedited and formatted. The final version may differ from this version.

agonist fragment of TBPB, VCP794, appeared less biased towards the $[Ca^{2+}]_i$ mobilisation pathway relative to the ERK1/2 pathway when compared to the parent compound.

The normalised responses of each agonist for the activation of $[Ca^{2+}]_i$ mobilisation and ERK1/2 phosphorylation, at equimolar concentrations, were replotted against each other to construct a bias plot (Figure 6C; (Gregory et al., 2010)). From this, an evident difference in the profile of VCP794 was observed, reflecting the agonist's greater preference for ERK1/2 phosphorylation relative to ACh and TBPB. Complementing this qualitative visualisation of bias, a quantitative measure of bias was determined through application of an operational model of agonism (equation 2) to the agonist concentration-response curves of these three agonists from both of these assays (Evans et al., 2011; Kenakin et al., 2012). This provided quantification of the transduction coefficient of each agonist's intrinsic efficacy for signal transduction in the system. These values are compiled in Table 4. The calculated bias between the $[Ca^{2+}]_i$ mobilisation transduction coefficient to the transduction coefficient for ERK1/2 phosphorylation, are depicted in Figure 6D. Statistical comparison of the bias factors for the three agonists found significant differences between the bias factor of VCP794 to those of ACh and TBPB, whilst no significant difference was determined between the values of ACh and TBPB ($p<0.05$, one-way ANOVA, post-hoc Bonferroni test).

In contrast, VCP813 did not exhibit any agonism for $[Ca^{2+}]_i$ mobilisation and ERK1/2 phosphorylation responses at the M_1 mAChR. Subsequent interaction studies screening non-agonist fragment compounds revealed that VCP813 exhibited appreciable antagonism of ACh responses in both signalling outputs studied (Figure 7A&B). This concentration-dependent reduction in ACh potency by VCP813 was well fitted by the Schild model, and allowed us to estimate the functional affinity of VCP813 (pA_2= 5.54 ± 0.04, Schild Slope= 1.14 ± 0.03).

Molecular Pharmacology Fast Forward. Published on June 24, 2013 as DOI: 10.1124/mol.113.087320
This article has not been copyedited and formatted. The final version may differ from this version.

Evidence for a competitive mode of interaction by fragments of TBPB

The identification of VCP813 as an antagonist afforded more extensive investigation into the mode of binding of this fragment compound through further functional interaction studies. Given the appreciable conservation of the molecular structure of its parent, it is probable that VCP813 interacts with the same novel binding domain as TBPB. As such, functional interaction studies were performed to determine the effect of VCP813 on TBPB-mediated $[Ca^{2+}]_i$ mobilisation responses at the M_1 mAChR. Like ACh, TBPB was similarly antagonised by VCP813 (Figure 7C). Not only were the data of the dextral displacement of the TBPB concentration-response curve well fitted to the Schild model (pA_2= 5.33 ± 0.10, Schild Slope= 1.38 ± 0.14), but the affinity estimate of VCP813 was also not significantly different from the estimated value from interaction studies with ACh in $[Ca^{2+}]_i$ mobilisation experiments ($p>0.05$, Student's t-test).

With the antagonism of ACh by VCP813 being consistent with a competitive mode of interaction with the orthosteric binding site, we sought to validate these observations through similar experiments with the orthosteric antagonist, atropine, on the $[Ca^{2+}]_i$ mobilisation elicited by ACh and TBPB (Figure 7D&E). As expected, atropine competitively antagonised ACh-mediated responses at the receptor, the data being well fitted to the Schild model (pA_2= 8.41 ± 0.09, Schild Slope= 0.97 ± 0.06). In contrast to the atropine-mediated depression of the maximal response by TBPB (Jones et al., 2008), we did not observe any change in the maximal responses of TBPB by the classical orthosteric antagonist, consistent with competitive antagonism (pA_2= 8.34 ± 0.01, Schild Slope= 1.11 ± 0.04). Further analysis found no significant difference between this affinity estimate and that determined from experiments with ACh ($p>0.05$, Student's t-test),

corroborating the hypothesis that TBPB may interact with the orthosteric site as well as suggesting that VCP813 can either interact with the orthosteric binding domain of the receptor or, alternatively, interact allosterically with high negative cooperativity.

Given that TBPB does not bind exclusively to the M_1 mAChR, we extended the functional studies of its fragments to the M_2, M_3 and M_4 mAChRs (Figure 8A-C). In comparison to the parent molecule, VCP794 activated both M_2 and M_4 mAChR-mediated ERK1/2 phosphorylation to the same maximum as ACh, but did not activate the M_3 mAChR. Subsequent interaction studies with ACh at the M_3 mAChR did not reveal any appreciable antagonism of ACh-mediated pERK1/2 phosphorylation response by VCP794 (data not shown). In the case of VCP813, similar to its profile at the M_1 mAChR, VCP813 did not exhibit agonist activity (Figure 8A-C) but antagonised ACh-mediated responses at all three receptor subtypes (Figure 8D-F). The antagonism of ACh by VCP813 fitted well to the Schild model (Table 5), consistent with a competitive interaction with the orthosteric agonist.

To better understand how these two fragment compounds engage with the mAChRs, additional equilibrium radioligand binding studies were conducted (Figure 9). Like its parent molecule, VCP794 displaced [^{3}H]-NMS from the M_1 mAChR. The lower binding affinity estimate of VCP794, compared to TBPB, is comparable to the difference in potency between the two agonists for M_1 mAChR-mediated $[Ca^{2+}]_i$ mobilisation, but not ERK1/2 phosphorylation. Similar binding affinity estimates were determined for the M_2 and M_4 mAChRs. Interestingly, compared to its binding at the M_1, M_2 and M_4 mAChRs, VCP794 exhibited a significantly lower affinity at the M_3 mAChR, to the extent that the highest concentration (10μM) investigated only displaced approximately 25% of [^{3}H]-NMS binding from the receptor.

Molecular Pharmacology Fast Forward. Published on June 24, 2013 as DOI: 10.1124/mol.113.087320
This article has not been copyedited and formatted. The final version may differ from this version.

VCP813 also inhibited [^{3}H]-NMS binding at these receptors, exhibiting similar binding affinity estimates across all the mAChR subtypes, albeit substantially lower compared to TBPB. This was consistent with the similar pA_2 values determined from previous functional experiments.

VCP813 interacts allosterically with the M_1 mAChR

Since VCP794 and VCP813 retain TBPB's ability to interact competitively with orthosteric ligands at the M_1 - M_4 mAChRs, we chose to investigate whether the molecular truncation of these ligands had led to the subtraction of the parent's allosteric nature. We investigated [^{3}H]-NMS dissociation in the presence and absence of VCP794 (100μM) and VCP813 (300μM) (Figure 10). These experiments determined that VCP794 did not significantly retard radioligand dissociation from the receptor (K_{off} = 0.213 ± 0.010 min^{-1}). VCP813 was able to significantly retard [^{3}H]-NMS dissociation from the M_1 mAChR (K_{off} = 0.151 ± 0.007 min^{-1}, p<0.05, F test vs atropine alone), demonstrating that the *ortho*-tolyl moiety of TBPB can engage with an allosteric binding site at the M_1 mAChR when the receptor has been pre-bound with [^{3}H]-NMS.

Molecular Pharmacology Fast Forward. Published on June 24, 2013 as DOI: 10.1124/mol.113.087320
This article has not been copyedited and formatted. The final version may differ from this version.

Discussion

The interest in the M_1 mAChR as a therapeutic target has led to the recent identification of a range of selective agonists for this receptor (Jones et al., 2008; Langmead et al., 2008a; Lebois et al., 2010; Spalding et al., 2002). Although the novel pharmacology of a number of these compounds has led to their classification as "allosteric" agonists, the evidence to support a purely allosteric mechanism of action for some of these compounds is equivocal (see Introduction). The M_1 mAChR-selective agonist, TBPB, is one such ligand and herein we provide evidence, using a molecular truncation approach, of a likely interaction with the orthosteric binding domain of the M_1 mAChR and a putative bitopic mechanism of action.

TBPB and its fragments display similar affinity for the M_2, M_3 and M_4 subtypes compared to the M_1 mAChR, with a maximal difference of approximately 3-fold (except for VCP794 at the M_3 mAChR). Additionally, both TBPB and VCP813 competitively antagonise ACh-mediated responses, in agreement with previous findings with TBPB (Lebois et al., 2010), suggesting that TBPB interacts with the highly homologous orthosteric binding domain of the receptor family. Interestingly, we also observed partial agonist activity of TBPB at the M_4 mAChR subtype, which has not been previously reported. This may explain the incomplete antagonism of ACh-stimulated activation of the M_4 mAChR observed by Lebois *et al.* (2010), and likely reflects the sensitivity of the cellular/biological system and end point studied compared to previous investigations. It also suggests TBPB exploits structural regions conserved between the M_1 and M_4 mAChR subtypes to elicit receptor activation. The apparently competitive behaviour of TBPB argues against a purely allosteric mechanism of agonism at the M_1 mAChR. Indeed, consideration of the evidence for a purely allosteric mechanism of action by TBPB is somewhat

inconclusive, with recent exploration of TBPB's SAR also uncovering competitive orthosteric pharmacology (Sheffler et al., 2013). In contrast to initial observations of non-competitive antagonism of TBPB by atropine (Jones et al., 2008), we observed competitive antagonism. Since we did not pre-equilibrate with atropine, this discrepancy likely reflects the limitations of non-equilibrium binding conditions of the assay (i.e., $[Ca^{2+}]_i$ mobilisation), whereby non-competitive antagonism can result from hemi-equilibria (Charlton and Vauquelin, 2010). Additionally, although TBPB retains agonist activity at various mutant receptors of the M_1 mAChR in which key orthosteric residues had been substituted for alanine (Jacobson et al., 2010; Jones et al., 2008), an interaction with the orthosteric binding domain by TBPB cannot be rejected, as it may still interact with other residues of the binding site.

TBPB is, however, capable of interacting with an allosteric site at the M_1 mAChR, as evidenced by its alteration of the dissociation kinetics of the orthosteric radioligand [^{3}H]-NMS demonstrated in our study and previously (Jacobson et al., 2010). Retardation of [^{3}H]-NMS dissociation by the fragment, VCP813, further supports an allosteric mechanism. Despite truncation of the parent molecule, VCP813 interacts competitively at the receptor with TBPB. Hence it is likely that these compounds, as well as sharing molecular structure, share the same allosteric site. However, although the retardation of radioligand dissociation is unequivocal evidence of an allosteric site interaction on a receptor already occupied by orthosteric ligand, this does not demonstrate whether TBPB prefers a purely allosteric mode of interaction with the free receptor. Indeed, this is a caveat to the detection of allosteric site interactions with this assay. Notably, the concentration of TBPB required to observe the allosteric effect on radioligand dissociation would likely saturate the receptor population in the absence of other ligands, based on our binding data. Additionally, a lower concentration of TBPB (50μM) has been reported to

have no effect on [^{3}H]-NMS dissociation (Sheffler et al., 2013), suggesting that a higher affinity orthosteric/bitopic interaction predominates over a much lower affinity (purely) allosteric interaction. In support of this notion, the retardation of [^{3}H]-NMS dissociation by the bitopic ligand McN-A-343, at the M_2 mAChR, has been defined at concentrations that are greater than its equilibrium dissociation constant (May et al., 2007; Valant et al., 2008). Thus, our findings support an orthosteric mode of interaction for TBPB, in addition to an established allosteric pharmacology at the M_1 mAChR. This dual orthosteric/allosteric behaviour is reconcilable with a bitopic mode of interaction.

Analysis of the pharmacological behaviour of various fragments of TBPB provides insight into its mechanism of action from its molecular structure. In particular, the distal *ortho*-tolyl moiety is possibly necessary for interaction with an allosteric site of the M_1 mAChR, whilst the lower benzoimidazolone end is required for interaction with the orthosteric site and receptor activation. In support of current beliefs is the finding that the fragment, VCP813, is able to retard [^{3}H]-NMS dissociation, despite an approximately 100-fold lower potency to displace the radioligand compared to TBPB. Furthermore, the possession of this aromatic moiety seems indispensable for the selective agonist activity, but not affinity, of TBPB for the M_1 mAChR, as demonstrated by our binding studies at other mAChR subtypes. Additionally, we found that VCP813 antagonised both ACh and TBPB with similar apparent affinities in a competitive-like manner. It is probable that the fragment retains a portion of the orthosteric binding moiety and is able to occupy part of the orthosteric binding domain like its parent molecule. Interestingly, VCP813 does not display appreciable binding selectivity for any mAChR subtype tested. It is possible that the allosteric domain engaged by the aromatic moiety of VCP813 (and TBPB), like several

Molecular Pharmacology Fast Forward. Published on June 24, 2013 as DOI: 10.1124/mol.113.087320
This article has not been copyedited and formatted. The final version may differ from this version.

prototypical allosteric modulators for mAChRs (Christopoulos et al., 1999; Ellis et al., 1991; Jakubíc et al., 1995), is structurally similar across the mAChR family.

The pharmacology of VCP794 also supports a common allosteric domain for the aromatic moiety. First, the absence of the distal *ortho*-tolyl moiety in VCP794 results in a bias of signalling towards ERK1/2 phosphorylation as compared to $[Ca^{2+}]_i$ mobilisation, relative to ACh, which is "restored" with the addition of the aromatic functionality in TBPB. Differences in stimulus bias engendered through simultaneous engagement of an allosteric and orthosteric site have been observed for other bitopic compounds as compared to their corresponding orthosteric pharmacophore constituent. For example, investigation of bitopic agonists for the adenosine A_1 receptor has reported a reversal of potencies between the stimulation of [^{35}S]-GTPγS binding and ERK1/2 phosphorylation relative to the individual orthosteric agonist component of the bitopic molecule (Narlawar et al., 2010). Second, there is a marked loss of agonist selectivity of VCP794 for the M_1 mAChR over other mAChR subtypes that can be related to the absence of the distal *ortho*-tolyl moiety of TBPB. This is consistent with previous studies of analogues of the TBPB molecular scaffold that possess or lack a distal aromatic moiety (Bridges et al., 2008; Budzik et al., 2010; Miller et al., 2008). It is noted that similar agonist studies have been previously conducted with VCP794 at each of the five mAChR subtypes, with a similar lack of subtype selectivity observed of the agonist (Budzik et al., 2010). Intriguingly, VCP794 displays poor binding affinity for the M_3 mAChR, which likely contributes to the lack of agonism observed at this receptor. This affinity is "restored" with the aromatic *ortho*-tolyl group extension of TBPB.

Given our findings, we propose that the *ortho*-tolyl moiety of TBPB engages with a common spatial allosteric domain of the mAChR family, whereby the engagement of this site provides

additional stabilising contact(s) with the mAChRs (such as the M_3 subtype). Furthermore, the structural differences within and proximal to this site between mAChR subtypes may engender different degrees of (negative) allosteric modulation of the agonist portion of the molecule. Indeed, such a mechanism of modulation of a ligand's own agonist responses has been demonstrated for the bitopic ligand, McN-A-343 at the M_2 mAChR (Valant et al., 2008). Consequently, this interaction with the orthosteric site of receptor is of importance for the translation and prediction of TBPB's pharmacology established *in vitro* to an *in vivo* setting. TBPB's orthosteric/bitopic interaction may provide insight into its lack of *in vivo* efficacy in reversing scopolamine-induced memory deficits in mice (Ma et al., 2009). Although activation of the M_1 mAChR is associated with memory and cognitive functions, a recent analysis of the antagonist occupancy of mAChRs in the brains of Rhesus macaques has suggested that blockade of M_2 mAChRs of the brain stem may also mediate memory deficits induced by muscarinic antagonists such as scopolamine (Yamamoto et al., 2011). Therefore, it is possible that the antagonism of non-M_1 mAChR subtypes by TBPB may negate any potential beneficial effects from M_1 mAChR activation in scopolamine-treated rats (Ma et al., 2009), with an analogous compound (with agonist activity at the other mAChR subtypes) able to reverse scopolamine-induced amnesia in rats (Budzik et al., 2010).

In conclusion, our results are consistent with a dual orthosteric/allosteric pharmacology of TBPB, most parsimoniously described by a concomitantly orthosteric/allosteric bitopic mechanism of action at the M_1 mAChR. These findings can provide a basis for reassessing the classification of other functionally selective agonists deemed to be solely allosteric.

Molecular Pharmacology Fast Forward. Published on June 24, 2013 as DOI: 10.1124/mol.113.087320
This article has not been copyedited and formatted. The final version may differ from this version.

Acknowledgments

We thank Drs. Michael Crouch and Ron Osmond (TGR Biosciences) for generously providing the ERK1/2 phosphorylation assay kit.

Molecular Pharmacology Fast Forward. Published on June 24, 2013 as DOI: 10.1124/mol.113.087320
This article has not been copyedited and formatted. The final version may differ from this version.

Authorship contributions

Participated in research design: *Keov, Valant, Lane, Sexton, Christopoulos*

Conducted experiments: *Keov, Valant*

Contributed new reagents or analytical tools: *Scammells, Devine*

Performed data analysis: *Keov, Valant, Lane, Christopoulos*

Wrote or contributed to writing of the manuscript: *Keov, Valant, Lane, Scammells, Devine Sexton, Christopoulos*

References

Arunlakshana O and Schild OH (1959) Some quantitative uses of drug antagonists. *Br J Pharmacol* **14**:48-58.

Avlani VA, Langmead CJ, Guida E, Wood MD, Tehan BG, Herdon HJ, Watson JM, Sexton PM and Christopoulos A (2010) Orthosteric and allosteric modes of interaction of novel selective agonists of the M_1 muscarinic acetylcholine receptor. *Mol Pharmacol* **78**(1):94-104.

Bodick NC, Offen WW, Levey AI, Cutler NR, Gauthier SG, Satlin A, Shannon HE, Tollefson GD, Rasmussen K, Bymaster FP, Hurley DJ, Potter WZ and Paul SM (1997) Effects of Xanomeline, a Selective Muscarinic Receptor Agonist, on Cognitive Function and Behavioral Symptoms in Alzheimer Disease. *Arch Neurol* **54**(4):465-473.

Bridges TM, Brady AE, Phillip Kennedy J, Nathan Daniels R, Miller NR, Kim K, Breininger ML, Gentry PR, Brogan JT, Jones CK, Jeffrey Conn P and Lindsley CW (2008) Synthesis and SAR of analogues of the M1 allosteric agonist TBPB. Part I: Exploration of alternative benzyl and privileged structure moieties. *Bioorg Med Chem Lett* **18**(20):5439-5442.

Budzik B, Garzya V, Shi D, Walker G, Woolley-Roberts M, Pardoe J, Lucas A, Tehan B, Rivero RA, Langmead CJ, Watson J, Wu Z, Forbes IT and Jin J (2010) Novel N-Substituted Benzimidazolones as Potent, Selective, CNS-Penetrant, and Orally Active M_1 mAChR Agonists. *ACS Med Chem Lett* **1**(6):244-248.

Chan WY, McKinzie DL, Bose S, Mitchell SN, Witkin JM, Thompson RC, Christopoulos A, Lazareno S, Birdsall NJM, Bymaster FP and Felder CC (2008) Allosteric modulation of the muscarinic M_4 receptor as an approach to treating schizophrenia. *Proc Natl Acad Sci U S A* **105**(31):10978-10983.

Charlton SJ and Vauquelin G (2010) Elusive equilibrium: the challenge of interpreting receptor pharmacology using calcium assays. *Br J Pharmacol* **161**(6):1250-1265.

Cheng Y-C and Prusoff WH (1973) Relationship between the inhibition constant (K_I) and the concentration of inhibitor which causes 50 per cent inhibition (I_{50}) of an enzymatic reaction. *Biochem Pharmacol* **22(**23):3099-3108.

Christopoulos A, Lanzafame A and Mitchelson F (1998) Allosteric Interactions at Muscarinic Cholinoceptors. *Clin Exp Pharmacol Physiol* **25**:185-194.

Christopoulos A, Loiacono R and Mitchelson F (1993) Binding of the muscarine receptor antagonist heptane-1,7-bis(dimethyl-3'-phthalimidopropyl) ammonium bromide at cholinoceptor sites. *Eur J Pharmacol: Mol Pharmacol* **246**(1):1-8.

Christopoulos A, Sorman JL, Mitchelson F and El-Fakahany EE (1999) Characterization of the Subtype Selectivity of the Allosteric Modulator Heptane-1,7-bis-(dimethyl-3'-phthalimidopropyl) Ammonium Bromide (C_7/3-phth) at Cloned Muscarinic Acetylcholine Receptors. *Biochem Pharmacol* **57**:171-179.

Clark AL and Mitchelson F (1976) The inhibitory effect of gallamine on muscarinic receptors. *Br J Pharmacol* **58**(3):323-331.

Conn PJ, Christopoulos A and Lindsley CW (2009) Allosteric modulators of GPCRs: a novel approach for the treatment of CNS disorders. *Nat Rev Drug Discov* **8**:41-54.

Crespo P, Xu N, Simonds WF and Gutkind JS (1994) Ras-dependent activation of MAP kinase pathway mediated by G-protein βγ subunits. *Nature* **369**(6479):418-420.

Digby, GJ, Utley, TJ, Lamsal, A, Sevel, C, Sheffler, DJ, Lebois, EP, Bridges, TM, Wood, MR, Niswender, CM, Lindsley, CW and PJ Conn (2012) Chemical modification of the M_1 agoist VU0364572 reveals molecular switches in pharmacology and a bitopic binding mode. *ACS Chem. Neurosci.*, **3:** 1025-1036.

Ellis J, Huyler J and Brann MR (1991) Allosteric regulation of cloned m1-m5 muscarinic receptor subtypes. *Biochem Pharmacol* **42**(10):1927-1932.

Evans BA, Broxton N, Merlin J, Sato M, Hutchinson DS, Christopoulos A and Summers RJ (2011) Quantification of Functional Selectivity at the Human α_{1A}-Adrenoceptor. *Mol Pharmacol* **79**(2):298-307.

Gregory KJ, Hall NE, Tobin AB, Sexton PM and Christopoulos A (2010) Identification of Orthosteric and Allosteric Site Mutations in M_2 Muscarinic Acetylcholine Receptors That Contribute to Ligand-selective Signaling Bias. *J Biol Chem* **285**(10):7459-7474.

Jacobson MA, Kreatsoulas C, Pascarella DM, O'Brien JA and Sur C (2010) The M1 Muscarinic Receptor Allosteric Agonists AC-42 and 1-[1'-(2-Methylbenzyl)-1,4'-bipiperidin-4-yl]-1,3-dihydro-2*H*-benzimidazol-2-one Bind to a Unique Site Distinct from the Acetylcholine Orthosteric Site. *Mol Pharmacol* **78**(4):648-657.

Jakubík J, Bacáková L, el-Fakahany EE and Tucek S (1995) Subtype selectivity of the positive allosteric action of alcuronium at cloned M_1-M_5 muscarinic acetylcholine receptors. *J Pharmacol Exp Ther* **274**(3):1077-1083.

Jones CK, Brady AE, Davis AA, Xiang Z, Bubser M, Tantawy MN, Kane AS, Bridges TM, Kennedy JP, Bradley SR, Peterson TE, Ansari MS, Baldwin RM, Kessler RM, Deutch AY, Lah JJ, Levey AI, Lindsley CW and Conn PJ (2008) Novel Selective Allosteric Activator of the M_1 Muscarinic Acetylcholine Receptor Regulates Amyloid Processing and Produces Antipsychotic-Like Activity in Rats. *J Neurosci* **28**(41):10422-10433.

Kenakin T, Watson C, Muniz-Medina V, Christopoulos A and Novick S (2012) A Simple Method for Quantifying Functional Selectivity and Agonist Bias. *ACS Chem Neurosci* **3**:193-203.

Kenakin T and Christopoulos (2013) Signalling bias in new drug discovery: detection, quantification and therapeutic impact. *Nature Rev Drug Discov* **12**: 205-216.

Keov P, Sexton PM and Christopoulos A (2011) Allosteric modulation of G protein-coupled receptors: A pharmacological perspective. *Neuropharmacology* **60**(1):24-35.

Langmead CJ, Austin NE, Branch CL, Brown JT, Buchanan KA, Davies CH, Forbes IT, Fry VAH, Hagan JJ, Herdon HJ, Jones GA, Jeggo R, Kew JNC, Mazzali A, Melarange R, Patel N, Pardoe J, Randall AD, Roberts C, Roopun A, Starr KR, Teriakidis A, Wood MD, Whittington M, Wu Z and Watson J (2008a) Characterization of a CNS penetrant, selective M_1 muscarinic receptor agonist, 77-LH-28-1. *Br J Pharmacol* **154**:1104-1115.

Langmead CJ, Watson J and Reavill C (2008b) Muscarinic acetylcholine receptors as CNS drug targets. *Pharmacol Ther* **117**:232-243.

Lebois EP, Bridges TM, Lewis LM, Dawson ES, Kane AS, Xiang Z, Jadhav SB, Yin H, Kennedy JP, Meiler J, Niswender CM, Jones CK, Conn PJ, Weaver CD and Lindsley CW (2010) Discovery and Characterization of Novel Subtype-Selective Allosteric

Agonists for the Investigation of M_1 Receptor Function in the Central Nervous System. *ACS Chem Neurosci* **1**:104-121.

Ma L, Seager MA, Wittmann M, Jacobson M, Bickel D, Burno M, Jones K, Graufelds VK, Xu G, Pearson M, McCampbell A, Gaspar R, Shughrue P, Danziger A, Regan C, Flick R, Pascarella D, Garson S, Doran S, Kreatsoulas C, Veng L, Lindsley CW, Shipe W, Kuduk S, Sur C, Kinney G, Seabrook GR and Ray WJ (2009) Selective activation of the M_1 muscarinic acetylcholine receptor achieved by allosteric potentiation. *Proc Natl Acad Sci U S A* **106**(37):15950-15955.

Marlo JE, Niswender CM, Days EL, Bridges TM, Xiang Y, Rodriguez AL, Shirey JK, Brady AE, Nalywajko T, Luo Q, Austin CA, Williams MB, Kim K, Williams R, Orton D, Brown HA, Lindsley CW, Weaver CD and Conn PJ (2009) Discovery and Characterization of Novel Allosteric Potentiators of M_1 Muscarinic Receptors Reveals Multiple Modes of Activity. *Mol Pharmacol* **75**(3):577-588.

May LT, Avlani VA, Langmead CJ, Herdon HJ, Wood MD, Sexton PM and Christopoulos A (2007) Structure-Function Studies of Allosteric Agonism at M_2 Muscarinic Acetylcholine Receptors. *Mol Pharmacol* **72**(2):463-476.

Miller NR, Daniels RN, Bridges TM, Brady AE, Conn PJ and Lindsley CW (2008) Synthesis and SAR of analogs of the M1 allosteric agonist TBPB. Part II: Amides, sulfonamides and ureas - The effect of capping the distal basic piperidine nitrogen. *Bioorg Med Chem Lett* **18**(20):5443-5447.

Narlawar R, Lane JR, Doddareddy M, Lin J, Brussee J and Ijzerman AP (2010) Hybrid Ortho/Allosteric Ligands for the Adenosine A_1 Receptor. *J Med Chem* **53**(8):3028-3037.

Nawaratne V, Leach K, Suratman N, Loiacono RE, Felder CC, Armbruster BN, Roth BL, Sexton PM and Christopoulos A (2008) New Insights into the Function of M_4 Muscarinic Acetylcholine Receptors Gained Using a Novel Allosteric Modulator and a DREADD (Designer Receptor Exclusively Activated by a Designer Drug). *Mol Pharmacol* **74**(4):1119-1131.

Rosenblum K, Futter M, Jones M, Hulme EC and Bliss TVP (2000) ERKI/II Regulation by the Muscarinic Acetylcholine Receptors in Neurons. *J Neurosci* **20**(3):977-985.

Sheffler DJ, Sevel C, Le U, Lovell KM, Tarr JC, Carrington SJS, Cho HP, Digby GJ, Niswender CM, Conn PJ, Hopkins CR, Wood MR and Lindsley CW (2013) Further exploration of M_1 allosteric agonists: Subtle structural changes abolish M_1 allosteric agonism and result in pan-mAChR orthosteric antagonism. *Bioorg Med Chem Lett* **23**(1):223-227.

Shekhar A, Potter WZ, Lightfoot J, Lienemann J, Dubé S, Mallinckrodt C, Bymaster FP, McKinzie DL and Felder CC (2008) Selective Muscarinic Receptor Agonist Xanomeline as a Novel Treatment Approach for Schizophrenia. *Am J Psychiatry* **165**(8):1033-1039.

Spalding TA, Trotter C, Skjarbak N, Messier TL, Currier EA, Burstein ES, Li D, Hacksell U and Brann MR (2002) Discovery of an Ectopic Activation Site on the M_1 Muscarinic Receptor. *Mol Pharmacol* **61**(6):1297-1302.

Stewart GD, Sexton PM and Christopoulos A (2010) Prediction of functionally selective allosteric interactions at an M_3 muscarinic acetylcholine receptor mutant using *Saccharomyces cerevisiae*. *Mol Pharmacol* **78**:205-214.

Stockton JM, Birdsall NJM, Burgen ASV and Hulme EC (1983) Modification of the Binding Properties of Muscarinic Receptors by Gallamine. *Mol Pharmacol* **23**:551-557.

Valant C, Gregory KJ, Hall NE, Scammells PJ, Lew MJ, Sexton PM and Christopoulos A (2008) A Novel Mechanism of G Protein-coupled Receptor Functional Selectivity. *J Biol Chem* **283**(43):29312-29321.

Ward SDC, Curtis CAM and Hulme EC (1999) Alanine-Scanning Mutagenesis of Transmembrane Domain 6 of the M_1 Muscarinic Acetylcholine Receptor Suggests that Tyr381 Plays Key Roles in Receptor Function. *Mol Pharmacol* **56**:1031-1041.

Yamamoto S, Nishiyama S, Kawamata M, Ohba H, Wakuda T, Takei N, Tsukada H and Domino EF (2011) Muscarinic Receptor Occupancy and Cognitive Impairment: A PET Study with [^{11}C](+)3-MPB and Scopolamine in Conscious Monkeys. *Neuropsychopharmacology* **36**(7):1455-1465.

Footnotes

This work was funded by the National Health and Medical Research Council of Australia (NHMRC) [Program Grant 519461] and Australian Research Council [Discovery Grant DP110100687]. A.C and P.M.S are Principal Research Fellows of the NHMRC. J.R.L. is a Career Development Fellow of the NHMRC. P.K. is a recipient of an Australian Postgraduate Award scholarship.

Molecular Pharmacology Fast Forward. Published on June 24, 2013 as DOI: 10.1124/mol.113.087320
This article has not been copyedited and formatted. The final version may differ from this version.

Legends for Figures

Figure 1. Structures of ACh, TBPB and truncated derivatives.

Figure 2. Inhibition of [^{3}H]-NMS binding by ACh or TBPB at the (A) M_1, (B) M_2, (C) M_3 or (D) M_4 mAChRs stably expressed in CHO FlpIn cell membranes. All experiments were performed against a *ca.* K_D concentration of rarioligand in the presence of 100μM (GppNHp) at 37°C for 1 h (M_1) or 30°C for 1.5 h (M_2-M_4). Non-specific binding was determined using 10 μM atropine. Data are plotted as mean ± S.E. from 3-9 independent experiments.

Figure 3. ERK1/2 phosphorylation elicited by ACh or TBPB via the (A) M_1, (B) M_2, (C) M_3 or (D) M_4 mAChR subtypes stably expressed in CHO FlpIn cells. Concentration-response curves were established at the time corresponding to peak ERK1/2 phosphorylation (3-5 mins) at 37°C. Data are plotted as mean ± S.E of 3-4 individual experiments.

Figure 4. TBPB antagonism of ACh-mediated ERK1/2 phosphorylation at the (A) M_2, (B) M_3 or (C) M_4 mAChR stably expressed in CHO FlpIn cells. TBPB was equilibrated for 30 min prior to (A, B) or co-added with (C) ACh. Other details as for Fig. 3. Data are plotted as mean ± S.E of 3-4 individual experiments.

Molecular Pharmacology Fast Forward. Published on June 24, 2013 as DOI: 10.1124/mol.113.087320
This article has not been copyedited and formatted. The final version may differ from this version.

Figure 5. Dissociation of [^{3}H]-NMS in the absence and presence of TBPB or C_7/3-phth. Membranes expressing the M_1 mAChR were pre-equilibrated with [^{3}H]-NMS for 60min at 37°C, followed by dissociation of the bound radioligand initiated with atropine (10μM) alone (control) or in the presence of the indicated compound. Data are depicted as mean ± S.E from 3-4 independent experiments. * *significantly different to atropine alone; p<0.05, F-test.*

Figure 6. Truncation of TBPB yields a fragment (VCP794) that retains agonist activity and is biased towards the activation of ERK1/2 phosphorylation. (A) $[Ca^{2+}]_i$ mobilisation and **(B)** ERK1/2 phosphorylation elicited by each agonist. Data normalised to the maximum response of ACh. **(C)** Bias plot of normalised responses (*y* ordinate response data) from (A) and (B) at equivalent concentrations for each agonist. Dashed line represents theoretical plot for equipotent responses. **(D)** Log. Bias Factors of agonists for the two pathways relative to ACh. Data are the mean ± S.E of 3-6 independent experiments. *$p<0.05$, *compared to ACh and TBPB (one-way ANOVA, post-hoc Bonferroni test).*

Figure 7. Fragments of TBPB are able to antagonise ACh-stimulated $[Ca^{2+}]_i$ mobilisation and ERK1/2 phosphorylation in a competitive manner. Concentration-response curves to (A, B & D) ACh or (C & F) TBPB alone and in the presence of **(A-C)** VCP813 or **(D-E)** atropine, with corresponding Schild regressions. Dashed lines on Schild regressions are indicative of a theoretical slope of 1. Data are plotted as mean ± S.E of 3-4 individual experiments.

Molecular Pharmacology Fast Forward. Published on June 24, 2013 as DOI: 10.1124/mol.113.087320
This article has not been copyedited and formatted. The final version may differ from this version.

Figure 8. M_2, M_3 or M_4 mAChR-mediated ERK1/2 phosphorylation in the presence of VCP794 or VCP813. ERK1/2 phosphorylation elicited by VCP794 or VCP813 at the **(A)** M_2, **(B)** M_3 and **(C)** M_4 mAChRs. TBPB and ACh curves (from Figure 2) are shown as reference. VCP813 concentration-dependent antagonism of ACh-mediated ERK1/2 phosphorylation at the **(D)** M_2, **(E)** M_3 and **(F)** M_4 mAChRs. Data are plotted as mean ± S.E of 3-6 individual experiments.

Figure 9. Inhibition of [^{3}H]-NMS binding by VCP794 or VCP813 at the (A) M_1 mAChR, (B) M_2 mAChR, (C) M_3 mAChR and (D) M_4 mAChR. Data are depicted as mean ± S.E of 3 independent experiments. Dashed curve fit of VCP794 in (C) based on assumption of complete displacement of [^{3}H]-NMS. TBPB inhibition curve (dotted line, from Figure 2) shown as reference. Other details as for Fig. 2.

Figure 10. **Dissociation of [^{3}H]-NMS in the absence and presence of truncated fragment compounds VCP794 or VCP813**. Data are depicted as mean ± S.E from 3-4 independent experiments. C_7/3-phth curve (dashed line; from Figure 5) shown as reference. Other details as for Fig. 5. * *significantly different to atropine alone; $p<0.05$, F-test*

Molecular Pharmacology Fast Forward. Published on June 24, 2013 as DOI: 10.1124/mol.113.087320
This article has not been copyedited and formatted. The final version may differ from this version.

Table 1. Affinity estimates for the competition between [^{3}H]NMS and ACh or TBPB at the M_1 mAChR. Values are expressed as negative logarithms of the equilibrium dissociation constant (pK_I), and represent mean ± S.E from 3 separate equilibrium binding experiments performed in triplicate.

	ACh	TBPB
M_1	4.05 ± 0.06	6.66 ± 0.02
M_2	5.64 ± 0.03	6.16 ± 0.02
M_3	4.41 ± 0.05	6.22 ± 0.07
M_4	4.74 ± 0.03	6.59 ± 0.04

Molecular Pharmacology Fast Forward. Published on June 24, 2013 as DOI: 10.1124/mol.113.087320
This article has not been copyedited and formatted. The final version may differ from this version.

Table 2. Potency and maximum agonist effect parameters of ACh and TBPB for mediating M_2, M_3 or M_4 mAChR-activated ERK1/2 phosphorylation. Parameters are mean ± S.E determined from at least 3 separate experiments.

	ACh		TBPB	
	pEC_{50} [a]	**E_{max} [b]**	**pEC_{50} [a]**	**E_{max} [b]**
M_1	7.83 ± 0.05	*100*	7.13 ± 0.01	101.7 ± 5.16
M_2	7.58 ± 0.13	*100*	*N.D.*	*N.D.*
M_3	7.94 ± 0.10	*100*	*N.D.*	*N.D.*
M_4	7.76 ± 0.10	*100*	6.82 ± 0.04	41.37 ± 0.76

[a] Negative logarithm of the concentration of agonist that elicits a response equal to 50% of the maximal response

[b] Maximal phosphorylation of ERK1/2 elicited by agonist as a percentage of the response elicited by ACh.

N.D. not determined

Molecular Pharmacology Fast Forward. Published on June 24, 2013 as DOI: 10.1124/mol.113.087320
This article has not been copyedited and formatted. The final version may differ from this version.

Table 3 TBPB potency estimates for antagonism of ACh-mediated ERK1/2 phosphorylation at the M_2, M_3 or M_4 mAChRs. Data are represented as mean ± S.E. of at least 3 experiments.

	M_2	M_3	M_4
pA_2 [a]	6.82 ± 0.15	6.61 ± 0.14	6.69 ± 0.11[b]
Schild Slope	1.39 ± 0.09	1.24 ± 0.10	2.00 ± 0.15[b]

[a] Negative logarithm of the molar concentration of antagonist that makes it necessary to double the concentration of agonist needed to elicit the original response.

[b] Values obtained through Schild analysis with no constraint of the baseline or maxima of concentration response curves

Table 4. Agonist transduction coefficients ($Log_{10}(\tau/K_A)$), normalized transduction coefficients ($\Delta Log_{10}(\tau/K_A)$), and bias factors ($\Delta\Delta Log_{10}(\tau/K_A)$) for $[Ca^{2+}]_i$ mobilisation and ERK1/2 phosphorylation at the M_1 mAChR.

	$[Ca^{2+}]_i$ mobilisation		ERK1/2 phosphorylation		LogBias Factor [a] $[Ca^{2+}]_i$ - ERK1/2
	$Log_{10}(\tau/K_A)$	$\Delta Log_{10}(\tau/K_A)$	$Log_{10}(\tau/K_A)$	$\Delta Log_{10}(\tau/K_A)$	$\Delta\Delta Log_{10}(\tau/K_A)$
ACh	8.97 ± 0.04	0.00 ± 0.05	7.84 ± 0.03	0.00 ± 0.04	0.00 ± 0.07 (1.00)
TBPB	8.37 ± 0.04	-0.61 ± 0.06	7.09 ± 0.03	-0.73 ± 0.04	0.12 ± 0.07 (1.30)
VCP794	7.88 ± 0.06	-1.09 ± 0.07	7.59 ± 0.03	-0.22 ± 0.04	-0.87 ± 0.09 (0.14)*

* $p<0.01$, one-way ANOVA, compared to ACh and TBPB

[a] Antilogarithm of the bias factor shown in parentheses

Molecular Pharmacology Fast Forward. Published on June 24, 2013 as DOI: 10.1124/mol.113.087320
This article has not been copyedited and formatted. The final version may differ from this version.

Table 5. Antagonist potency estimates of VCP813 on ACh-mediated $[Ca^{2+}]_i$ mobilisation.

Parameters are mean ± S.E determined from at least 3 separate experiments.

	M_1	M_2	M_3	M_4
pA_2 [a]	5.10 ± 0.06	5.37 ± 0.06	5.46 ± 0.1[c]	5.40 ± 0.11
Schild Slope	1.13 ± 0.06	2.04 ± 0.06	1.48 ± 0.18[c]	1.83 ± 0.26

[a] Negative logarithm of the molar concentration of antagonist that makes it necessary to double the concentration of agonist needed to elicit the original response.

[b] Values obtained through Schild analysis with no constraint of the baseline or maxima of concentration response curves

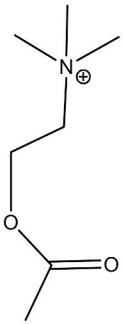

ACh

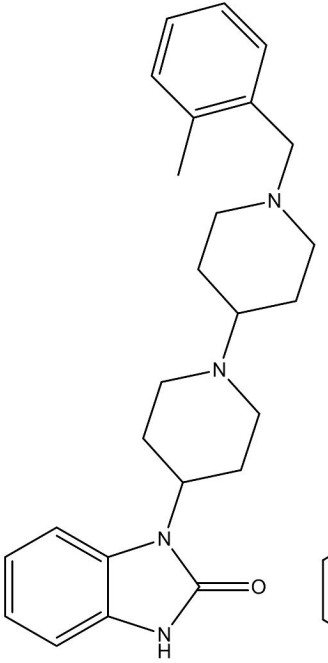

TBPB

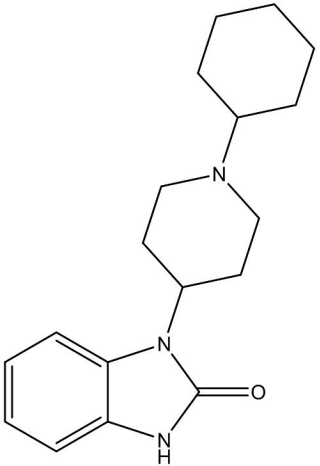

VCP794

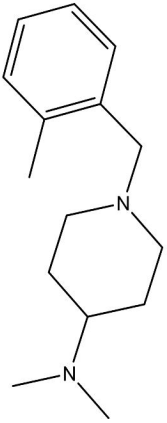

VCP813

Figure 1

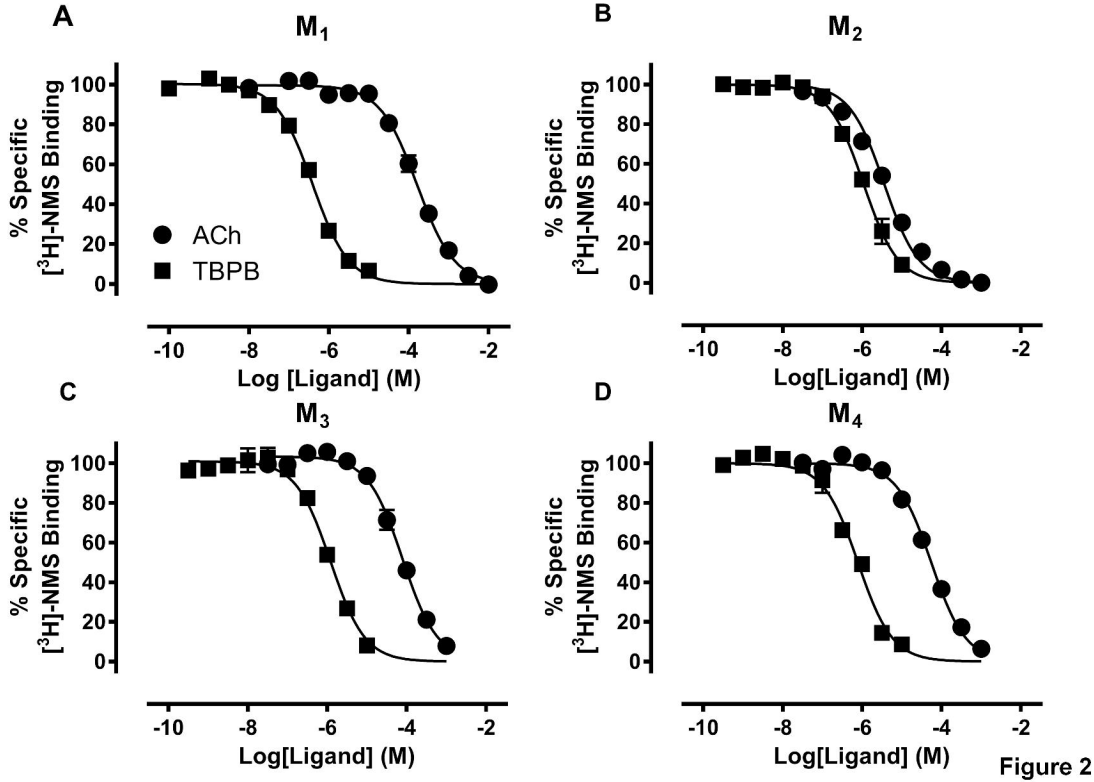
A
M1
% Specific
[3H]-NMS Binding
100
80
60
40
20
0
ACh
TBPB
-10
-8
-6
-4
-2
Log [Ligand] (M)
B
M2
% Specific
[3H]-NMS Binding
Log[Ligand] (M)
C
M3
% Specific
[3H]-NMS Binding
Log[Ligand] (M)
D
M4
% Specific
[3H]-NMS Binding
Log[Ligand] (M)

Figure 2

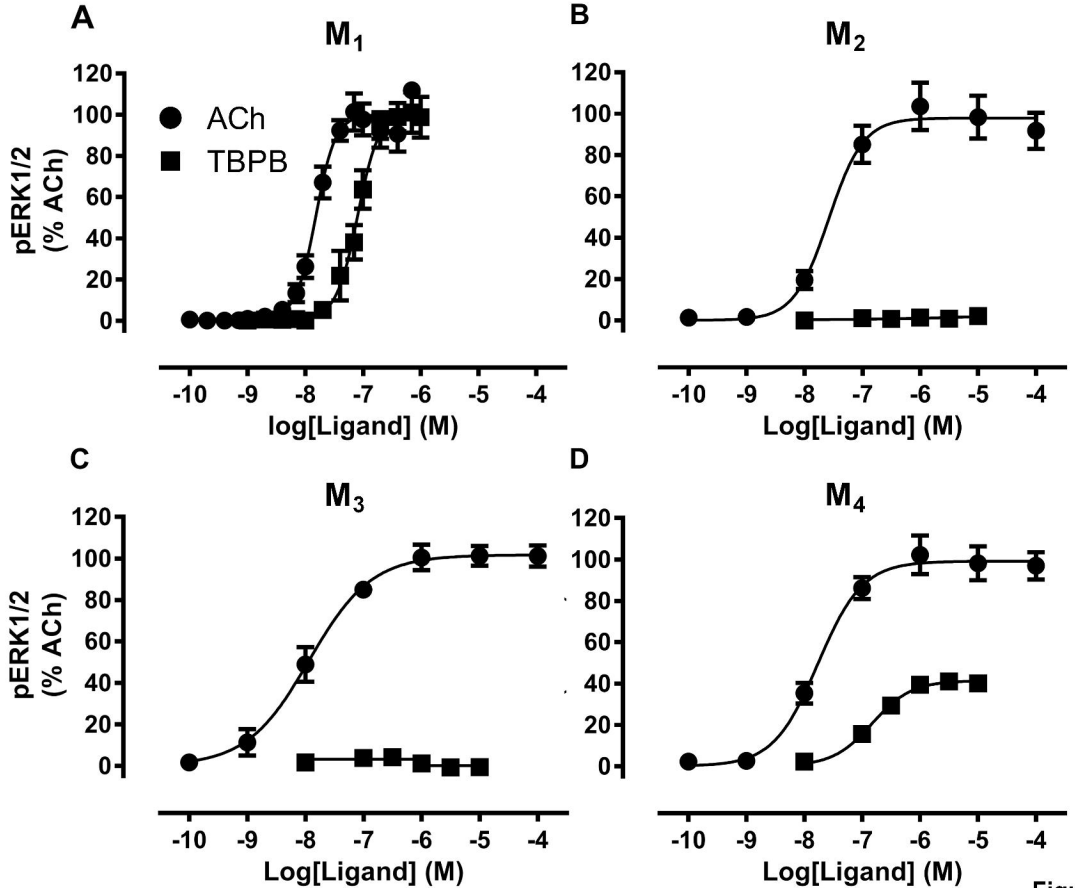
A
M1
ACh
TBPB
pERK1/2
(% ACh)
120
100
80
60
40
20
0
-10 -9 -8 -7 -6 -5 -4
log[Ligand] (M)
B
M2
Log[Ligand] (M)
C
M3
Log[Ligand] (M)
D
M4
Log[Ligand] (M)

Figure 3

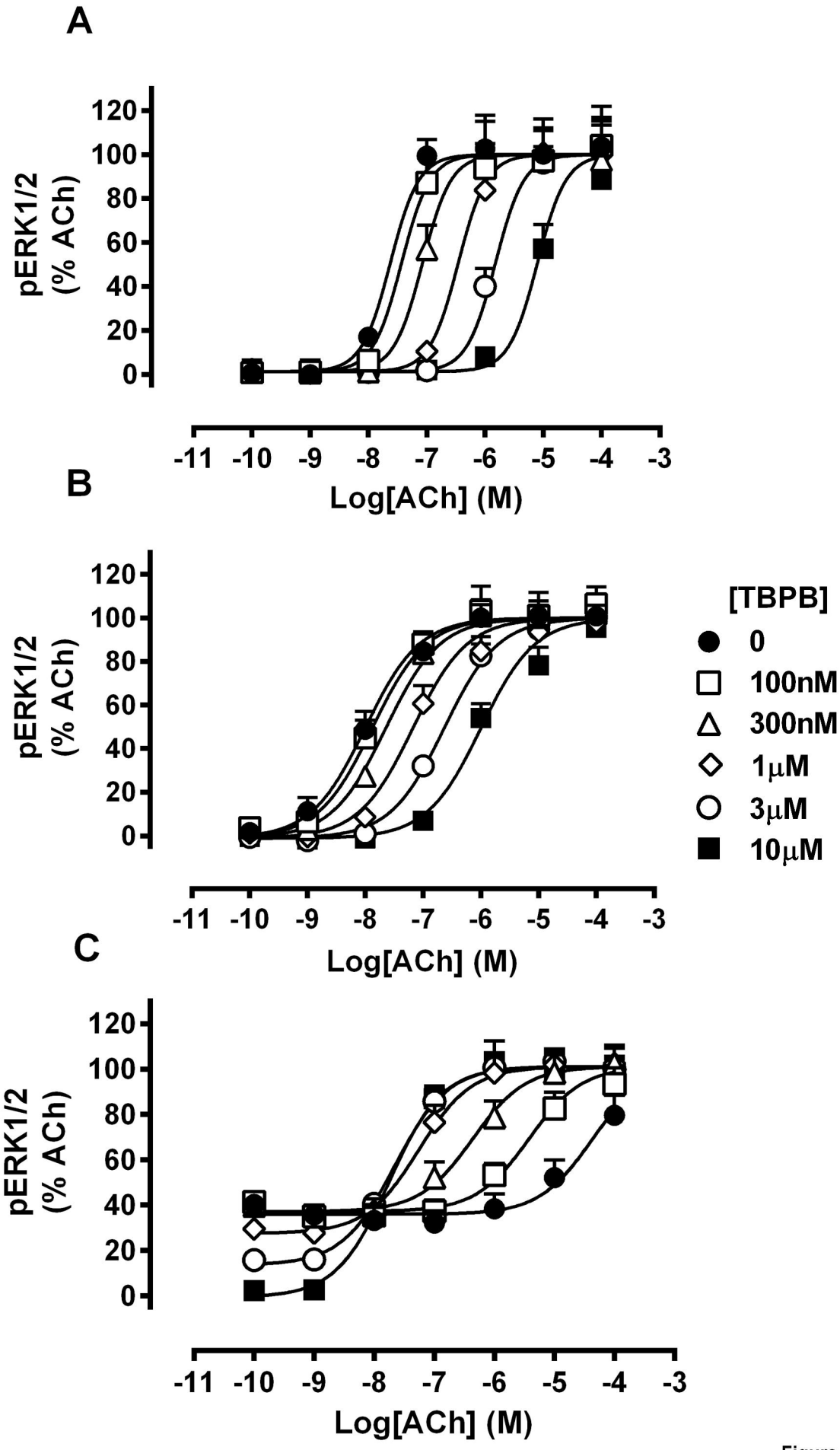
A
pERK1/2
(% ACh)
120
100
80
60
40
20
0
-11 -10 -9 -8 -7 -6 -5 -4 -3
Log[ACh] (M)
B
pERK1/2
(% ACh)
120
100
80
60
40
20
0
-11 -10 -9 -8 -7 -6 -5 -4 -3
Log[ACh] (M)
[TBPB]
0
100nM
300nM
1μM
3μM
10μM
C
pERK1/2
(% ACh)
120
100
80
60
40
20
0
-11 -10 -9 -8 -7 -6 -5 -4 -3
Log[ACh] (M)

Figure 4

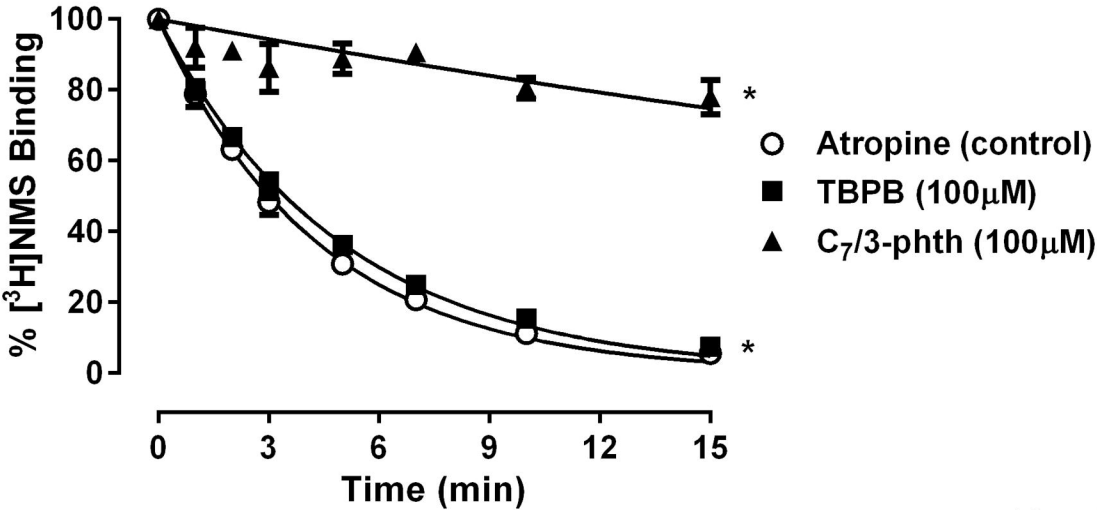
% [3H]NMS Binding
100
80
60
40
20
0
0
3
6
9
12
15
Time (min)
*
*
Atropine (control)
TBPB (100μM)
C7/3-phth (100μM)

Figure 5

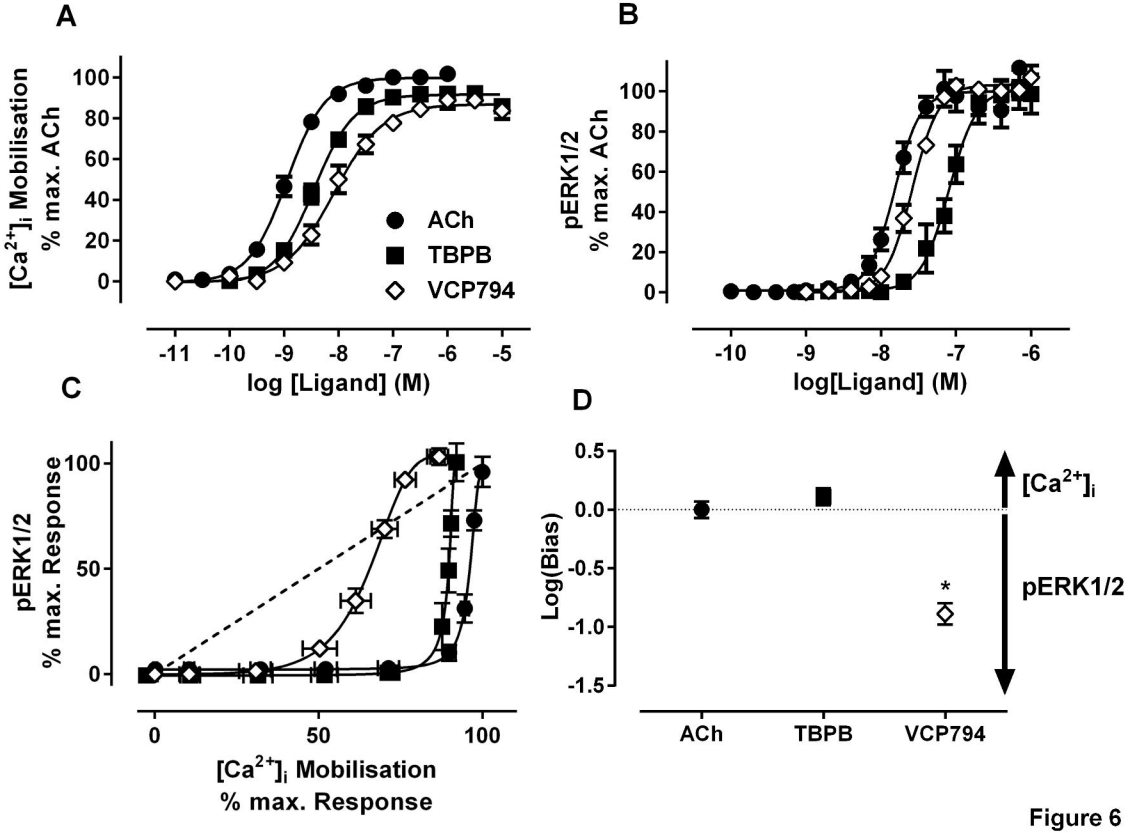
A
[Ca2+]i Mobilisation
% max. ACh
100
80
60
40
20
0
ACh
TBPB
VCP794
-11
-10
-9
-8
-7
-6
-5
log [Ligand] (M)
B
pERK1/2
% max. ACh
100
80
60
40
20
0
-10
-9
-8
-7
-6
log[Ligand] (M)
C
pERK1/2
% max. Response
100
50
0
0
50
100
[Ca2+]i Mobilisation
% max. Response
D
Log(Bias)
0.5
0.0
-0.5
-1.0
-1.5
*
[Ca2+]i
pERK1/2
ACh
TBPB
VCP794

Figure 6

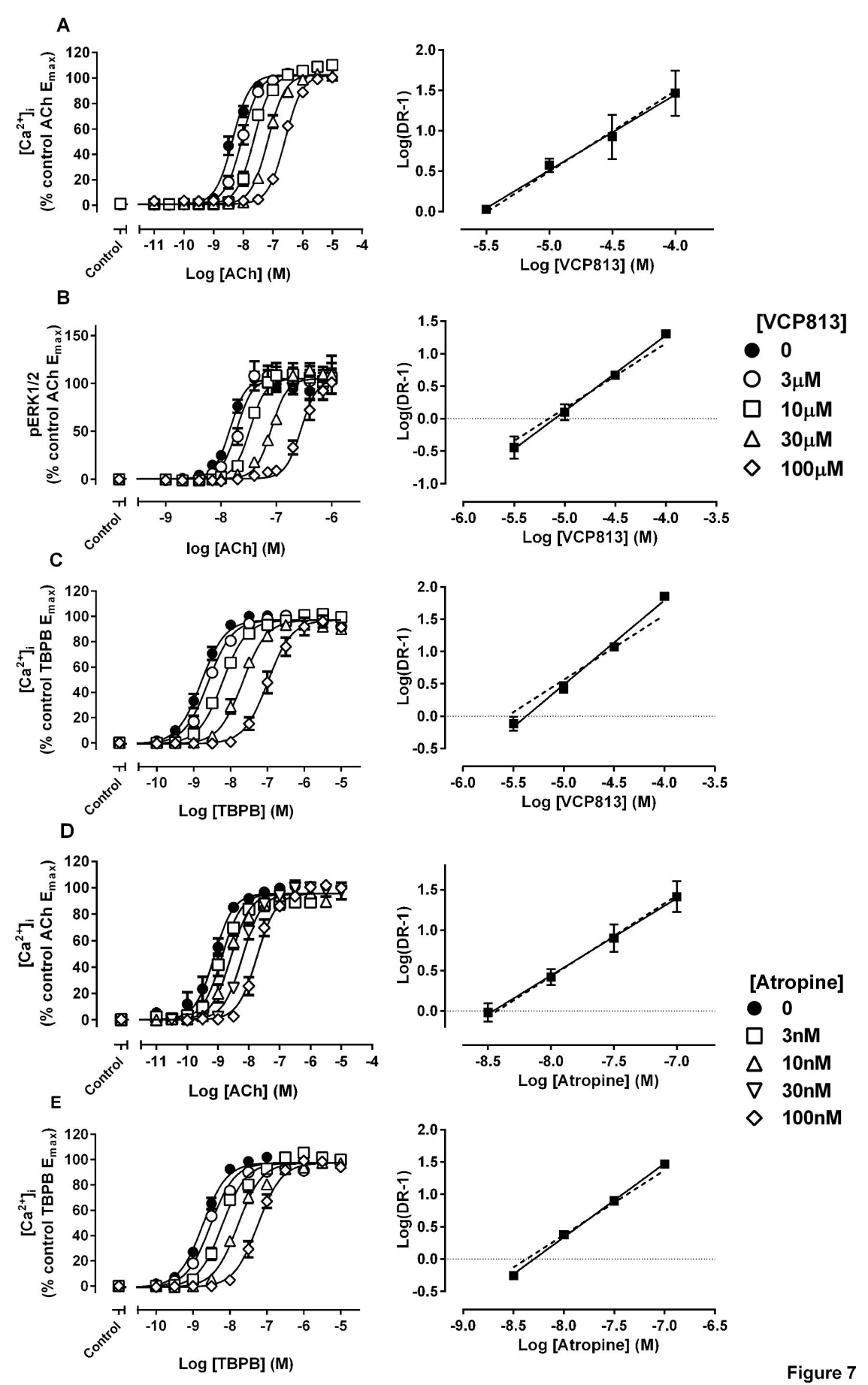
A
[Ca2+]i (% control ACh Emax)
Control
Log [ACh] (M)
Log(DR-1)
Log [VCP813] (M)
B
pERK1/2 (% control ACh Emax)
log [ACh] (M)
[VCP813]
0
3μM
10μM
30μM
100μM
C
[Ca2+]i (% control TBPB Emax)
Log [TBPB] (M)
D
Log [Atropine] (M)
[Atropine]
0
3nM
10nM
30nM
100nM
E

Figure 7

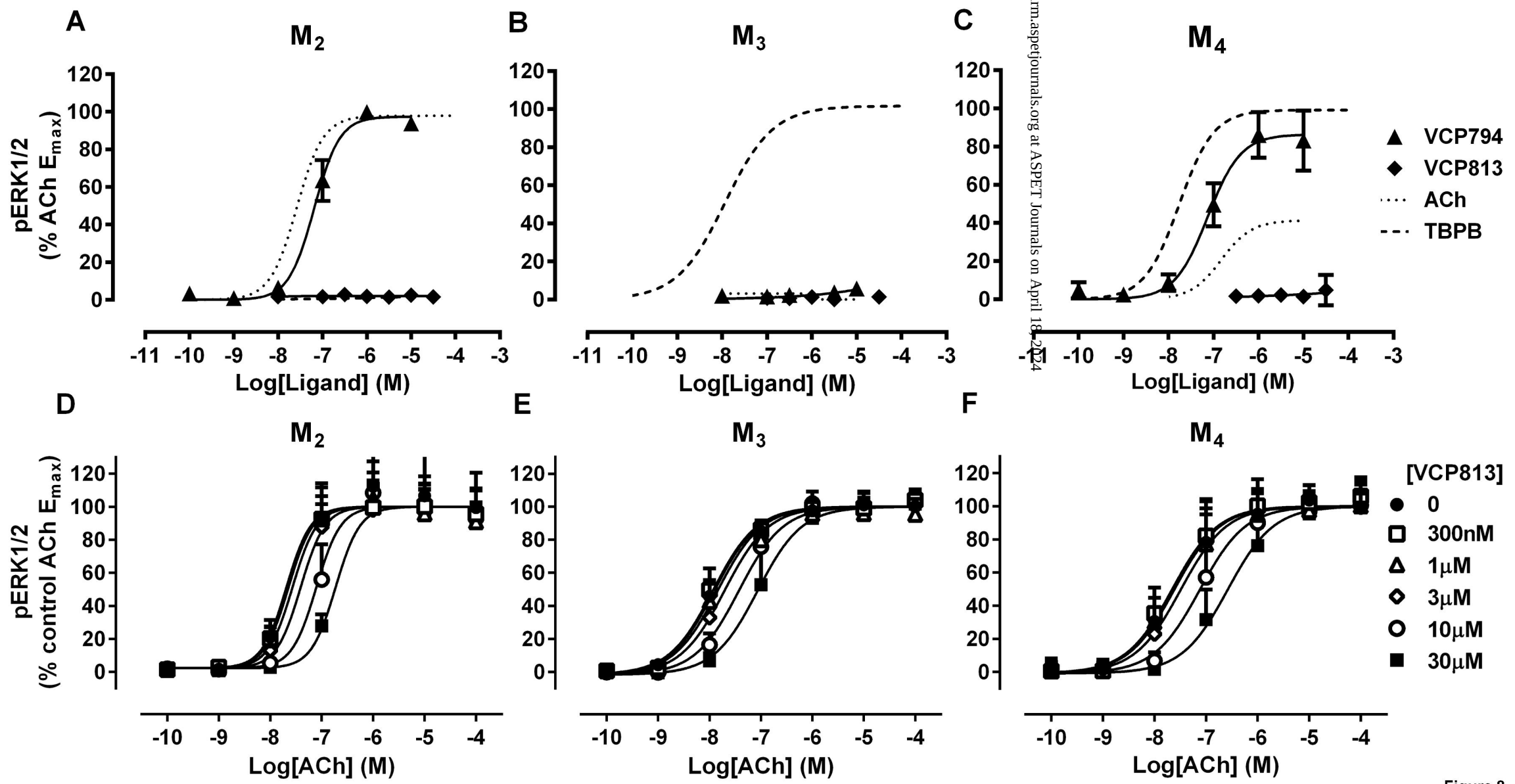

Figure 8

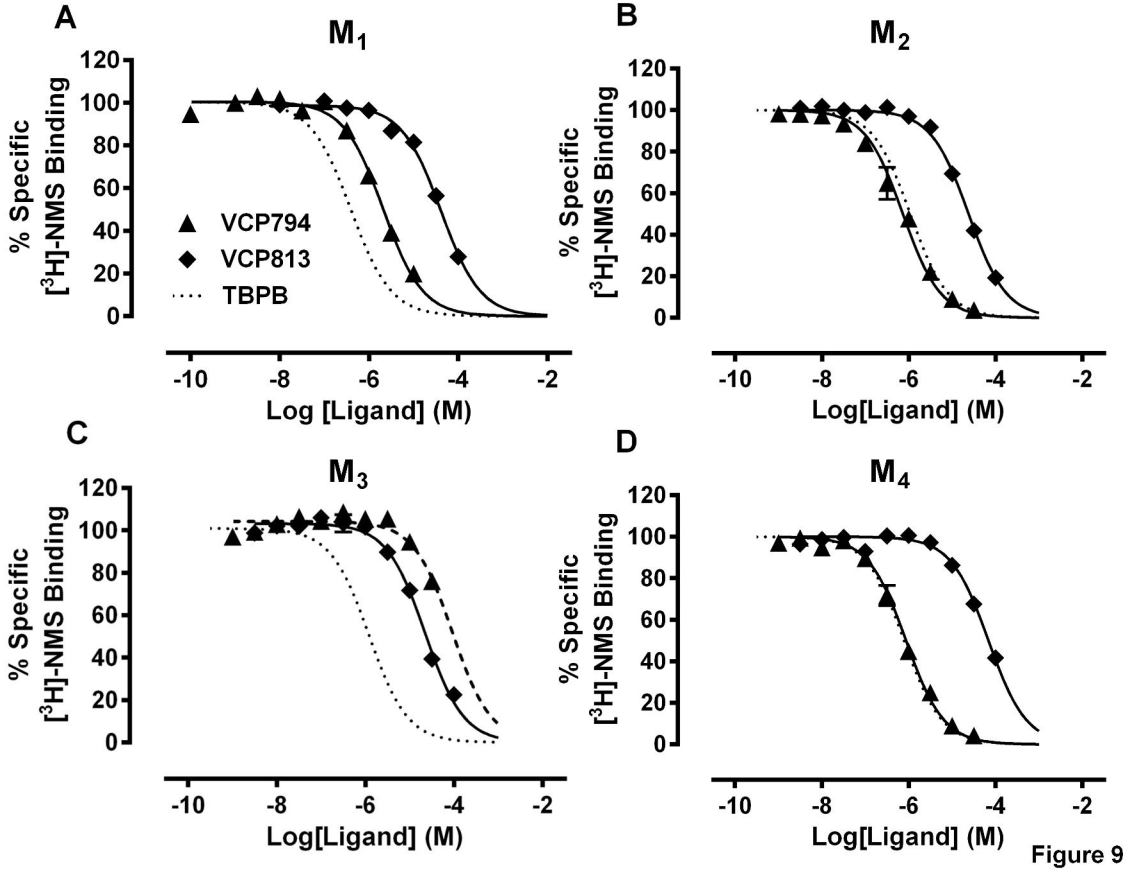
A
M1
B
M2
C
M3
D
M4
% Specific
[3H]-NMS Binding
120
100
80
60
40
20
0
VCP794
VCP813
TBPB
-10
-8
-6
-4
-2
Log [Ligand] (M)
Log[Ligand] (M)

Figure 9

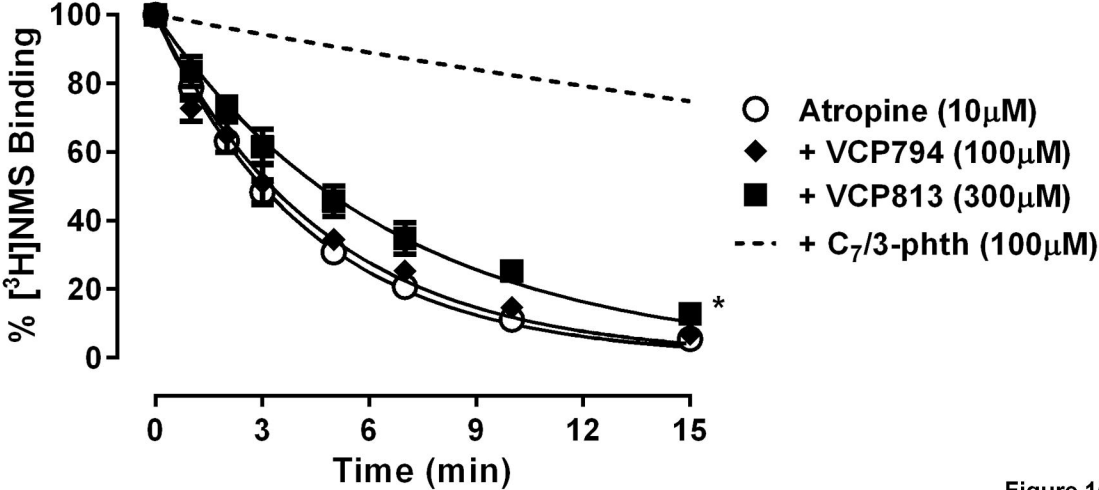
100
80
60
40
20
0
% [3H]NMS Binding
0
3
6
9
12
15
Time (min)
*
Atropine (10μM)
+ VCP794 (100μM)
+ VCP813 (300μM)
+ C7/3-phth (100μM)

Figure 10